separations

MDPI

*Article*

# A Comparative Study of Bulk and Surface Nanobubbles in Enhancing Coal Flotation

**Hua Han [1,2,3], Yan Li [1,2,3], Bingfei Yang [1,2,3,*], Xiaowei Zhang [1,2,3,*], Wenhui Ma [1] and Wenbo Li [1]**

[1] School of Gemology and Materials, Hebei GEO University, Shijiazhuang 050031, China
[2] Engineering Research Center for Silicate Solid Waste Resource Utilization of Hebei Province, Hebei GEO University, Shijiazhuang 050031, China
[3] Hebei Key Laboratory of Green Development of Rock and Mineral Materials, Hebei GEO University, Shijiazhuang 050031, China
* Correspondence: w_center@126.com (B.Y.); hl3751@126.com (X.Z.)

**Abstract**

Nanobubbles have been widely recognized for enhancing fine particle flotation, yet the distinct roles of bulk nanobubbles (BNBs) and surface nanobubbles (SNBs) remain poorly understood. This study systematically compares the effects of BNBs and SNBs on coal flotation using a unified hydrodynamic cavitation platform—BNBs generated in clean water and SNBs generated directly on particle surfaces by cavitating the coal slurry. Flotation tests, kinetics analysis, contact angle measurements, and agglomeration observations were conducted across varying reagent dosages and pulp concentrations. The results show that BNBs have negligible influence on flotation performance across all tested conditions, whereas SNBs significantly improve combustible recovery, particularly at low collector and frother dosages, where combustible recovery increased from 71.52% to 82.03% at a low collector dosage and from 45.03% to 61.71% at a low frother dosage. SNBs also enhanced flotation kinetics, increasing the rate constant from 1.83 to 2.10 $min^{-1}$, and improved surface hydrophobicity and fine particle agglomeration, which likely account for the observed enhancement in flotation performance. Notably, although BNBs showed measurable increases in contact angle on model substrates, their inability to effectively anchor onto coal particles under real flotation conditions makes them practically ineffective. This study provides critical insights into the likely dominant role of SNBs in nanobubble-assisted flotation and offers guidance for process optimization in fine coal beneficiation.

**Keywords:** bulk nanobubbles; surface nanobubbles; coal flotation; hydrodynamic cavitation; particle agglomeration; flotation kinetics

Check for updates

Academic Editor: Shuling Gao

Received: 21 August 2026
Revised: 30 September 2026
Accepted: 10 October 2026
Published: 13 October 2026

**Copyright:** © 2026 by the authors. Licensee MDPI, Basel, Switzerland. This article is an open access article distributed under the terms and conditions of the Creative Commons Attribution (CC BY) license.

## 1. Introduction

Flotation is the most effective technology of mineral processing to separate valuable minerals from gangue based on differences in surface hydrophobicity [1]. However, as high-grade and easily accessible ores continue to be depleted, it has become necessary to process increasingly complex, low-grade, and finely disseminated mineral resources. This trend necessitates finer grinding to achieve mineral liberation, resulting in a significant proportion of particles in the micro-size range. The recovery of fine and ultrafine particles remains a persistent and critical challenge in the mining industry, as their low mass, high specific surface area, and low collision probability with conventional-sized flotation bubbles lead to low recovery, high reagent consumption, poor flotation kinetics, and increased processing costs [2].

Nanobubble (NB) flotation technology has emerged as an effective method to overcome the limitations of traditional fine particle flotation techniques [3]. Nanobubbles, which are ultrafine gaseous bubbles with a diameter of less than 1 μm, possess unique physical and chemical properties, including high specific surface area, long-term stability, large contact angle, and high negative surface charge [4–6]. Numerous studies have demonstrated that the introduction of NBs can significantly improve the flotation performance in various mineral systems. In chalcopyrite flotation, the presence of micro-nano bubbles increased the recovery rate of ultrafine particles by 16–21%, while reducing the consumption of collectors by up to 75% [7]. For coal flotation, nanobubbles increase the combustible recovery by 5–23%, and reduce the content of clean coal ash by 1–3% [8], but also significantly improved flotation kinetics across different size fractions, with the most pronounced enhancement observed for fine particles [9]. In graphite flotation, compared with conventional flotation, nanobubble flotation increased the recovery by 5% and reduced the lower limit of flotation particle size to 2 μm [10]. Similarly, NBs reduced the consumption of both collectors and depressants by more than 50% while maintaining high recovery [11].

Recent studies have significantly advanced the understanding of the mechanisms underlying NB-enhanced flotation. NBs promote the formation of stable hydrophobic aggregates during flotation, effectively increasing the apparent particle size and thereby improving the collision probability with conventional bubbles [12]. The aggregation mechanism is mainly attributed to the "nanobubble bridging capillary force," where surface-attached NBs on adjacent hydrophobic particles coalesce to form gas bridges that generate a strong, long-range attractive force [13]. In addition, surface nanobubbles (SNBs) can significantly reduce the induction time for bubble–particle attachment by disrupting the hydration film and providing preferential sites for microbubble coalescence [14]. Molecular dynamics simulations have further revealed the "flash expansion" phenomenon of gas bridges on hydrophobic surfaces, which rapidly expand and enhance capillary attraction [15].

Nanobubbles can be classified into two main types based on their location: bulk nanobubbles (BNBs) exist in a dispersed and stable state in the liquid phase, while surface nanobubbles (SNBs) are nucleated at the solid–liquid interface [16]. It should be noted that BNBs can adsorb onto hydrophobic surfaces and transform into SNBs; theoretically, SNBs can also detach from the mineral surface and form BNBs under specific hydrodynamic conditions [17]. BNBs generated by cavitation may enhance flotation efficiency through two mechanisms: (i) they serve as a reservoir that supplies SNBs to particle surfaces, and (ii) they increase the bubble number density in the pulp, thereby improving the particle–bubble collision probability [18]. SNBs play a more direct role in the flotation process, as they selectively nucleate on hydrophobic surfaces and are proposed to act as "secondary collectors" by enhancing the local surface hydrophobicity. More importantly, they form capillary bridges between adjacent particles, generating strong attractive forces and thereby promoting stable hydrophobic aggregation [19–21].

The mechanism of action of different types of NBs remains unclear, and some studies have reported seemingly contradictory experimental results regarding the role of NBs in flotation. For instance, Wang et al. [22] reported that NBs enhance collector adsorption on mineral surfaces, leading to improved hydrophobicity of the particle surface and increased flotation recovery. Conversely, Ren et al. [23] demonstrated that NBs compete with collectors for adsorption sites, reducing collector uptake while still improving flotation performance. A reduction in reagent adsorption and an increase in recovery by NBs were observed in the flotation of both rutile and cassiterite [24,25]. These observations suggest that the relative importance of BNBs versus SNBs may vary depending on the generation method and mineral system.

Furthermore, the effects of nanobubbles on particle aggregation and surface wettability have been investigated across a range of minerals and experimental conditions, as summarized in Table 1. These studies employed various NB generation methods, including temperature difference, hydrodynamic cavitation, and micro-nano bubble generators. The particle sizes ranged from ultrafine (<10 μm) to fine (<100 μm), and the bubble sizes varied from approximately 50 nm to several micrometers. Contact angle measurement, atomic force microscopy (AFM), focused beam reflectance measurement (FBRM), and flotation kinetics were among the techniques used. Despite these efforts, most studies either focused on a single NB type or used generation methods that produce both BNBs and SNBs simultaneously, making it difficult to decouple their individual contributions. Consequently, the relative roles of BNBs and SNBs in promoting particle aggregation and modifying surface wettability remain unclear.

**Table 1.** Representative studies on the effects of nanobubbles on particle aggregation and surface wettability.

| Reference | Mineral/Ore | NB Generation Method | Particle Size | Bubble Size | Investigation Technique | Main Results |
|---|---|---|---|---|---|---|
| Heidari et al., 2024 [1] | copper | Hydrodynamic cavitation | $d_{80}$ = 150 μm | ~600 nm (fresh); 5 μm after 25 d | Flotation; dynamic light scattering; electrophoretic light scattering | Recovery +24.5% (mono-mineral), +7% (ore); collector adsorption +73.8% |
| Jiang et al., 2025 [3] | Ultrafine coal | Hydrodynamic cavitation | $d_{50}$ = 14.46 μm | 117–136.7 nm | Nanoparticle tracking analysis; Atomic force microscope; Laser particle size analyzer; High-speed camera imaging | Increased aggregate size; improved recovery and rate |
| Ahmadi et al., 2014 [7] | Chalcopyrite | Hydrodynamic cavitation | −38 + 5 μm | $d_{50}$ = 13.24 μm | Laser Particle Size Analyzer; Zeta-potential measurements; Surface tension measurements; | Recovery +16–21%; collector −75% |
| Ma et al., 2025 [10] | Graphite | Temperature difference | <38 μm | none | Laser particle size analyzer; Zeta potential measurement; XPS | Average size +13 μm; recovery +5%; carbon +1% |
| Sobhy et al., 2026 [11] | Fluorite | Hydrodynamic cavitation | $d_{95}$ = 150 μm | none | Density Functional Theory; flotation | Recovery +7.2%; reagent −50% |
| Dutta et al., 2025 [18] | Glass particles | Nanopore diffusion | $d_{50}$ = 35.2 μm | 70–200 nm | Nanoparticle tracking analysis; Dynamic light scattering; microscopy | Recovery +11%; collector −50%, frother −60% |
| Ge et al., 2025 [26] | Hematite/chlorite | Hydrodynamic cavitation | −74 + 38 μm | 25–65 μm; Nanobubbles account for 7.8 % | Pixact online bubble tese; Zeta potential measurement; flotation | Recovery +13.69%; Separation efficiency +35.06% |
| Wang et al., 2022 [22] | Molybdenum | Hydrodynamic cavitation | −15 μm | ~250 nm | Dynamic light scattering; Zeta potential measurement; Turbidity tests; Contact angle | Ultrafine molybdenite recovery +15.17%; enhanced aggregation |
| Ren et al., 2023 [23] | Cassiterite/calcite | Micro-nano bubble generator | <200 μm | <10 μm | Dynamic light scattering; Zeta potential measurement; Adsorption capacity measurements | Selective aggregation; reduced reagent; improved recovery |
| Zhang et al., 2025 [27] | Ilmenite | Micro-nano bubble generator | $d_{90}$ = 26.13 μm | 124.4 nm and $6.95 \times 10^7$ /mL | Nanoparticle tracking analysis; In situ particle size measurement; Atomic force microscope | Recovery +14.53%; enhanced agglomeration |

A critical gap in current understanding is the lack of systematic comparative studies that can identify which type of nanobubble dominates under practical flotation conditions, thereby providing a rational basis for optimizing NB generation and application. Identifying the dominant contributor is therefore not an end in itself, but a prerequisite for the rational design of NB-assisted flotation processes.

This study evaluates and compares the effects of BNBs and SNBs on the flotation of fine coal particles using cavitation. BNBs are generated by cavitating deionized water in the

absence of particles, while SNBs are generated by cavitating the coal slurry, where bubbles nucleate directly on hydrophobic particle surfaces. The distinction enables the selective production of each NB type, allowing their individual contributions to be distinguished. Flotation performance is evaluated through reagent optimization and kinetic studies, while the mechanisms are elucidated via contact angle measurements, collector adsorption measurements, and particle aggregation analysis. We hypothesize that SNBs dominate over BNBs in enhancing fine coal flotation; this study aims to test this hypothesis and provide insights for NB-assisted flotation design.

## 2. Materials and Methods

### *2.1. Materials*

#### 2.1.1. Coal Sample

The flotation feed used in this study was collected from the Bailong Coal Preparation Plant, located in Huozhou, Shanxi Province, China. The as-received sample was subjected to proximate analysis on an air-dry basis, with the results summarized in Table 1.

The proximate analysis and particle size distribution of the sample are presented in Tables 2 and 3, respectively. As shown, 31.57% of the particles are finer than 0.045 mm, and the sample has an ash content of 28.12%, confirming its typical fine coal nature, which poses significant challenges for conventional flotation. The mineralogical composition was characterized by X-ray diffraction (XRD), with kaolinite and quartz identified as the dominant gangue minerals. These fundamental properties are consistent with those reported for samples from the same source in our previous investigation [9]. Nevertheless, the present work employs a freshly collected batch to ensure the representativeness of subsequent flotation tests.

**Table 2.** Proximate analysis of the coal sample (air-dry basis, wt%).

| $M_{ad}$ (%) | $V_{ad}$ (%) | $FC_{ad}$ (%) | $A_{ad}$ (%) |
|---|---|---|---|
| 1.37 | 27.96 | 46.45 | 24.22 |

$M_{ad}$—moisture content, $V_{ad}$—volatile content, $FC_{ad}$—fixed carbon content, and $A_{ad}$—ash content.

**Table 3.** Particle size distribution of the coal sample.

| Size Fraction (mm) | Weight (%) | Ash Content (%) |
|---|---|---|
| −0.5 + 0.25 | 25.68 | 23.12 |
| −0.25 + 0.125 | 20.42 | 21.95 |
| −0.125 + 0.074 | 13.38 | 22.25 |
| −0.074 + 0.045 | 8.95 | 21.82 |
| −0.045 | 31.57 | 28.12 |
| Total | 100.00 | 24.22 |

#### 2.1.2. Preparation of Model Hydrophobic Substrates for Contact Angle Measurements

Hydrophobic substrates with controlled wettability were prepared to investigate the effect of surface hydrophobicity on nanobubble behavior and to provide reproducible surfaces for contact angle measurements. Coal surfaces are heterogeneous and rough, which leads to poorly reproducible contact angle data; therefore, model substrates were used to isolate the effect of surface wettability.

Highly polished glass slides were used as substrates for contact angle measurements to minimize the influence of surface roughness on the test results. Prior to hydrophobization, the glass slides were sequentially cleaned in an ultrasonic bath with ethanol and deionized water for 15 min each, then dried under a nitrogen stream. The cleaned slides were vertically immersed in a beaker containing a silane coupling agent (octadecyltrichlorosilane,

OTS, Sinopharm Chemical Reagent Co., Ltd., Shanghai, China) solution of varying concentrations, and the solution was stirred at constant temperature for 30 min. After the reaction, the slides were removed, thoroughly rinsed with deionized water, and dried at 60 °C for 2 h. Three substrate types with distinct wettability were obtained by adjusting the silane concentration and reaction time: weakly hydrophobic (approximately 30°), moderately hydrophobic (approximately 60°), and strongly hydrophobic (approximately 90°). For each substrate, contact angle measurements were performed at three different positions using the captive bubble method, and the average value was recorded to ensure reproducibility.

#### 2.1.3. Different Density Fractions of Coal Sample

For density fractionation, raw coal from the Bailong Coal Preparation Plant was crushed to below 3 mm and screened to obtain the −3 + 0.5 mm fraction, which was then subjected to float-sink tests using $ZnCl_2$ solutions of varying densities. Five density fractions were collected: −1.4 g/cm$^3$, 1.4–1.5 g/cm$^3$, 1.5–1.6 g/cm$^3$, 1.6–1.8 g/cm$^3$, and +1.8 g/cm$^3$. Each density fraction was subsequently crushed to below 74 μm, and the corresponding ash contents are presented in Table 4. For agglomeration experiments, the −45 μm fraction of each density fraction was selected as the test material, with the −1.4 g/cm$^3$, 1.4–1.8 g/cm$^3$, and +1.8 g/cm$^3$ fractions representing low-, medium-, and high-density coal samples, respectively.

**Table 4.** Ash content of different size fractions and density coal fractions.

| Densimetric Fraction (g/cm$^3$) | Ash Content (%) |
|---|---|
| −1.4 | 6.23 |
| 1.4–1.5 | 12.37 |
| 1.5–1.6 | 23.84 |
| 1.6–1.8 | 37.53 |
| +1.8 | 70.08 |

### *2.2. Methods*

#### 2.2.1. Flotation

The NB flotation experimental system is schematically illustrated in Figure 1. The apparatus consists of a conditioning tank, a peristaltic pump, a venturi tube, and a mechanical flotation cell. In a typical operation, the coal sample and tap water were introduced into the conditioning tank and agitated for 1 min to ensure thorough dispersion. The resulting suspension, together with entrained air, was then circulated through the venturi tube by a peristaltic pump for 1 min, with the throat velocity and aeration rate set at 16 m/s and 75 mL/min, respectively. The conditioned slurry was then transferred to the flotation cell. The subsequent flotation procedure was similar to that of conventional flotation, except that the conditioning time before collector (kerosene, Sinopharm Chemical Reagent Co., Ltd., Shanghai, China) and frother (sec-octanol Sinopharm Chemical Reagent Co., Ltd., Shanghai, China) reagent addition was reduced to 30 s to minimize the loss of pre-generated nanobubbles. The present study focuses on the comparative evaluation between BNB and SNB systems.

#### 2.2.2. Nanobubble Size Analysis Tests

The size distribution and number concentration of bulk nanobubbles were characterized using a nanoparticle tracking analyzer (NTA, NS300, Malvern Panalytical, Malvern, UK) following the procedure described by Montazeri et al. [6] with minor modifications. The instrument and its software interface are shown in Figure 2. The Tyndall effect was used as a preliminary visual indication of nanobubble presence, as reported previously. The

sample was introduced into the instrument chamber via a syringe pump at a constant flow rate of 100 µL/min. For each measurement, a 60 s video was recorded with the camera level set at 14 and the detection threshold at 5. At least five independent measurements were performed for each sample by moving the measurement position to different locations within the cell to ensure statistical representativeness. The recorded videos were analyzed using NTA 3.4 software, which tracks the Brownian motion of individual particles and calculates their hydrodynamic diameter based on the Stokes-Einstein equation. All measurements were performed at room temperature (approximately 25 °C). The results are reported as mean ± standard deviation (SD) from the replicate measurements, providing both the size distribution profiles and the absolute concentration (particles/mL) of the nanobubbles.

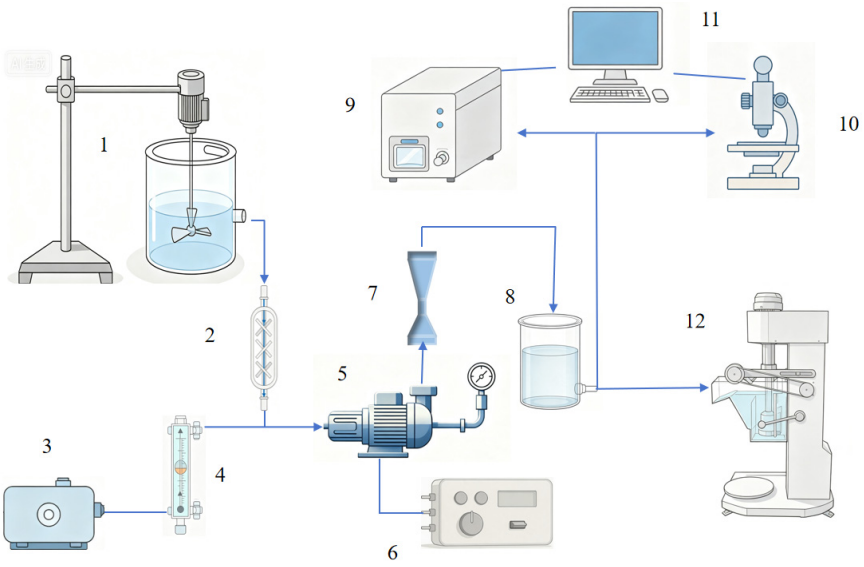
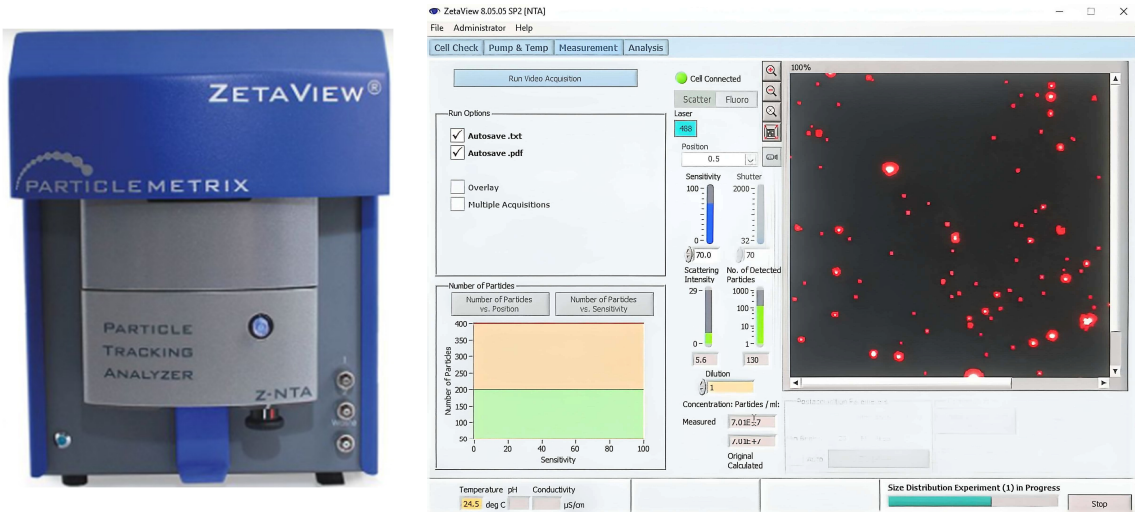



**Figure 1.** Schematic diagram of experimental apparatus: (1) agitator; (2) static mixer; (3) air pump; (4) gas flowmeter; (5) water pump; (6) controller; (7) venturi tube; (8) container; (9) NTA; (10) microscope; (11) computer; (12) flotation machine.




(**a**) (**b**)

**Figure 2.** Nanoparticle tracking analysis: (**a**) instrument photograph; (**b**) software interface.

### 2.2.3. Contact Angle Measurements on Model Hydrophobic Substrates

The hydrophobicity of the model hydrophobic substrate surfaces was characterized by the captive bubble method, with the experimental setup schematically illustrated in Figure 3a. In this method, both the solid substrate and the gas phase (air) are initially

immersed in the liquid phase (deionized water) prior to contact, and the measurement is performed with the bubble adhering to the underside of the substrate. A 5 μL air bubble was generated using a microsyringe and carefully injected onto the surface of the prepared substrate, which was placed in an organic glass cell. After the bubble was allowed to stabilize and form a three-phase contact line on the substrate (Figure 3b), the image was captured with a high-resolution camera. The contact angle was measured using image analysis software (ImageJ 1.54g), with the angle measured on both the left and right sides of the bubble, and the average value recorded. For each condition, at least three replicate measurements were performed on different locations of the substrate surface, and the mean value and standard deviation were reported. Hydrophobized glass slides were used as model substrates instead of coal, because coal surfaces are heterogeneous and rough, leading to poorly reproducible contact angle measurements. This approach is commonly adopted in nanobubble research to isolate the effect of surface wettability.

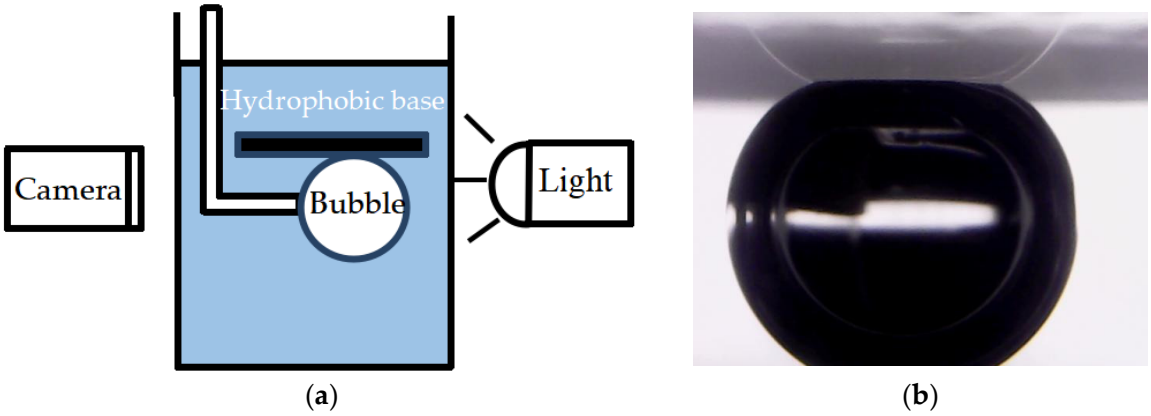



**Figure 3.** Contact angle measurement on a model hydrophobic substrate under the influence of nanobubbles: (**a**) experimental setup; (**b**) captured image of a bubble on the substrate.

#### 2.2.4. Observation of Aggregation of Coal Particles

A video-enhanced image analyzer equipped with a CCD industrial camera (Shaanxi Microvision Digital Image Technology Co., Ltd., Xi'an, China)was employed to observe the aggregation and dispersion behavior of fine coal particles. Coal samples with particle sizes below 45 μm, obtained from the float-sink tests at different density fractions (−1.4 g/cm$^3$, 1.4–1.8 g/cm$^3$, and +1.8 g/cm$^3$), were used. In each test, 0.5 g of coal sample was accurately weighed and transferred to a 250 mL beaker containing 200 mL of deionized water. The suspension was stirred on a magnetic stirrer at 500 rpm for 3 min to ensure thorough dispersion and wetting of the particles. After stirring, a small droplet of the slurry was transferred onto a glass slide using a pipette, and the slide was placed under the image analyzer for observation. The nanobubble preparation conditions were identical to those described in the adsorption tests. For each condition, at least five randomly selected fields of view were captured to ensure statistical representativeness of the observed aggregation behavior.

#### 2.2.5. Statistical Analysis

All flotation experiments, contact angle measurements, and kinetic tests were performed in triplicate. The results are presented as mean ± standard deviation (SD). Statistical comparisons among different conditions were performed using one-way analysis of variance (ANOVA) followed by Tukey's post hoc test. A $p$-value < 0.05 was considered statistically significant. The 95% confidence intervals were calculated using the t-distribution.

## 3. Results

### *3.1. Characterization of Nano-Bubbles Generated by Hydrodynamic Cavitation*

To verify the generation of nanobubbles via hydrodynamic cavitation, the Tyndall effect was employed as a preliminary indicator, as shown in Figure 4. In deionized water without any treatment (Figure 4a), no visible laser beam could be observed, indicating the absence of colloidal-sized scatterers. After hydrodynamic cavitation treatment in the absence of surfactant (Figure 4b–d), a distinct Tyndall cone became clearly visible, accompanied by a slight increase in solution turbidity. Upon standing, the turbidity gradually diminished (Figure 4c,d), while the Tyndall cone persisted, suggesting the presence of submicrometer scattering entities. Given the negligible impurity content in the deionized water, the observed colloidal entities are attributed to bulk nanobubbles generated during cavitation.

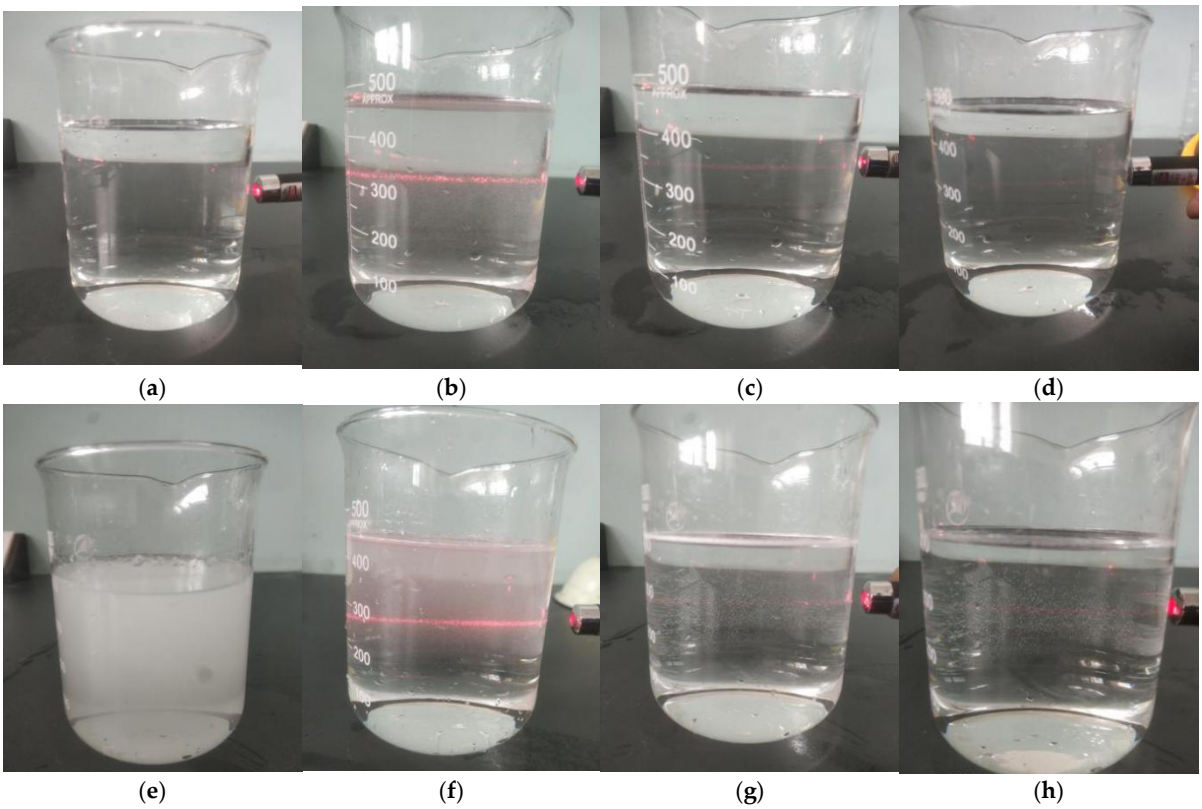



**Figure 4.** (**a**) The deionized pure water; (**b**) hydrodynamic cavitation without surfactant; (**c**) hydrodynamic cavitation without surfactant after 1 min; (**d**) hydrodynamic cavitation without surfactant after 5 min; (**e**) hydrodynamic cavitation with surfactant; (**f**) hydrodynamic cavitation with surfactant after 0.5 min; (**g**) hydrodynamic cavitation with surfactant after 1 min; (**h**) hydrodynamic cavitation with surfactant after 5 min.

When sec-octanol was introduced as a surfactant prior to cavitation (Figure 4e–h), the solution exhibited a pronounced milky-white appearance immediately after treatment (Figure 4f). This turbidity is primarily attributed to the abundant generation of micron-sized bubbles, which rapidly rose to the surface and collapsed under buoyancy within a few minutes (Figure 4g,h). Notably, after the dissipation of micron-sized bubbles, a stable Tyndall cone remained observable in the supernatant (Figure 4h), confirming the persistent presence of nanobubbles. These observations are consistent with the established understanding that surfactant molecules reduce the surface tension at the gas–liquid interface, promoting the formation of finer bubbles during cavitation. The stability of the nanobubbles observed in this study is in good agreement with previous reports [15].

The size distribution and concentration of bulk nanobubbles in deionized water, both with and without hydrodynamic cavitation treatment, were characterized by NTA, and the results are presented in Figure 5. Untreated deionized water was first measured as a blank reference (Figure 5a). A measurable population of scatterers was already present in the untreated water, with an average concentration of approximately $7 \times 10^6$ particles/mL and a mean size of approximately 160 nm (Figure 5b,c). These background entities are likely attributable to dissolved gas aggregates or trace impurities commonly present in ultrapure water.

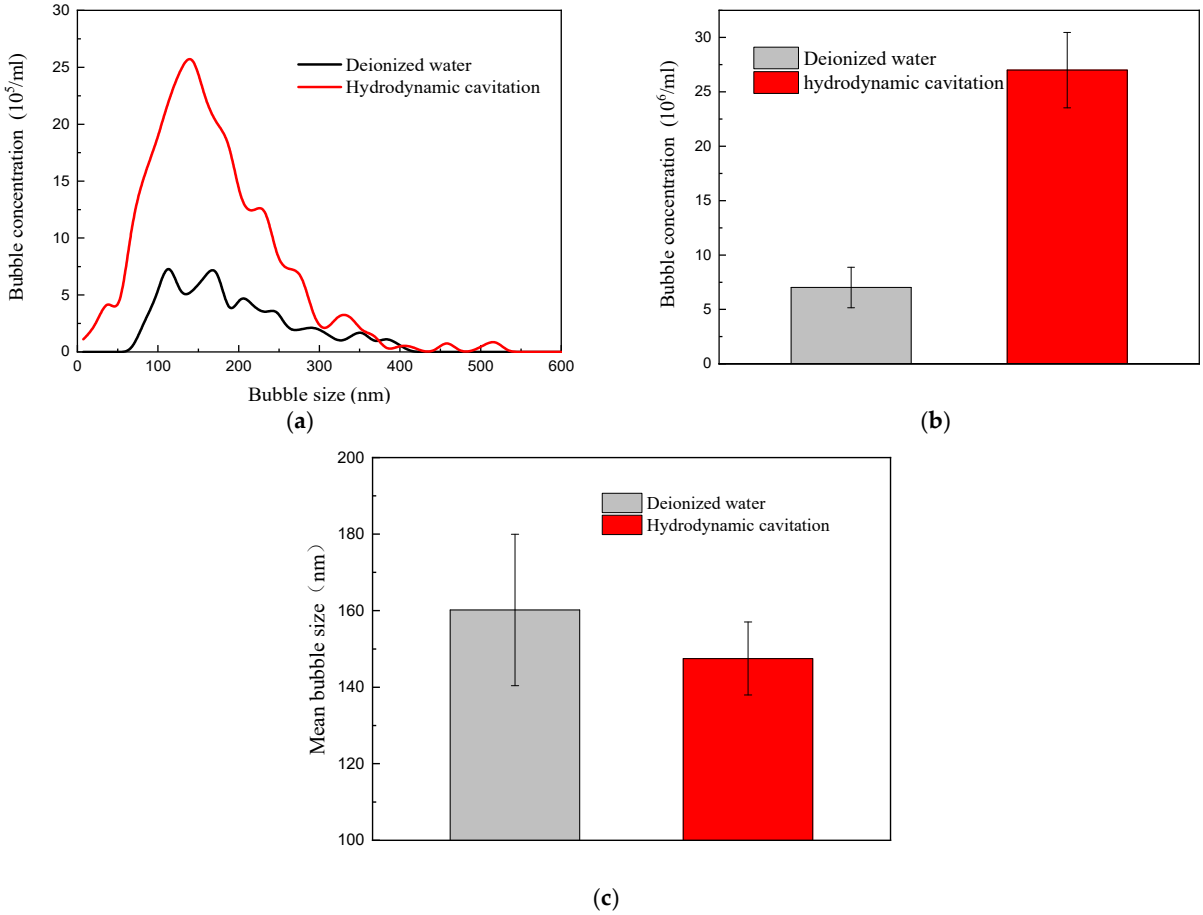



**Figure 5.** (**a**) The distribution curve of size and concentration of bulk nanobubbles in deionized pure water and deionized pure water after hydrodynamic cavitation; (**b**) the average concentrate of bulk nanobubbles in solution in two conditions; (**c**) the average size of bulk nanobubbles in solution in two conditions.

After hydrodynamic cavitation treatment, the solution was allowed to stand for 5 min before measurement to allow any transient microbubbles to rise and dissipate. The NTA results showed a substantial increase in bubble concentration to $2.7 \times 10^7$ particles/mL, accompanied by a slight reduction in mean size to 147 nm. The increase in number concentration confirms that hydrodynamic cavitation effectively promotes the formation of additional bulk nanobubbles, while the decrease in average size suggests that the cavitation process preferentially generates finer bubbles [6]. Notably, even after the dissipation of microbubbles, a stable population of nanobubbles remained detectable in the solution, consistent with their well-documented colloidal stability [16].

While NTA provides quantitative size and concentration data for bulk nanobubbles, direct AFM imaging of surface nanobubbles (SNBs) on coal surfaces remains challenging because of the heterogeneous and rough nature of coal particles. In our previous work [9],

we provided direct AFM evidence of SNB formation on a model hydrophobic substrate under the same hydrodynamic cavitation conditions (Figure 6).

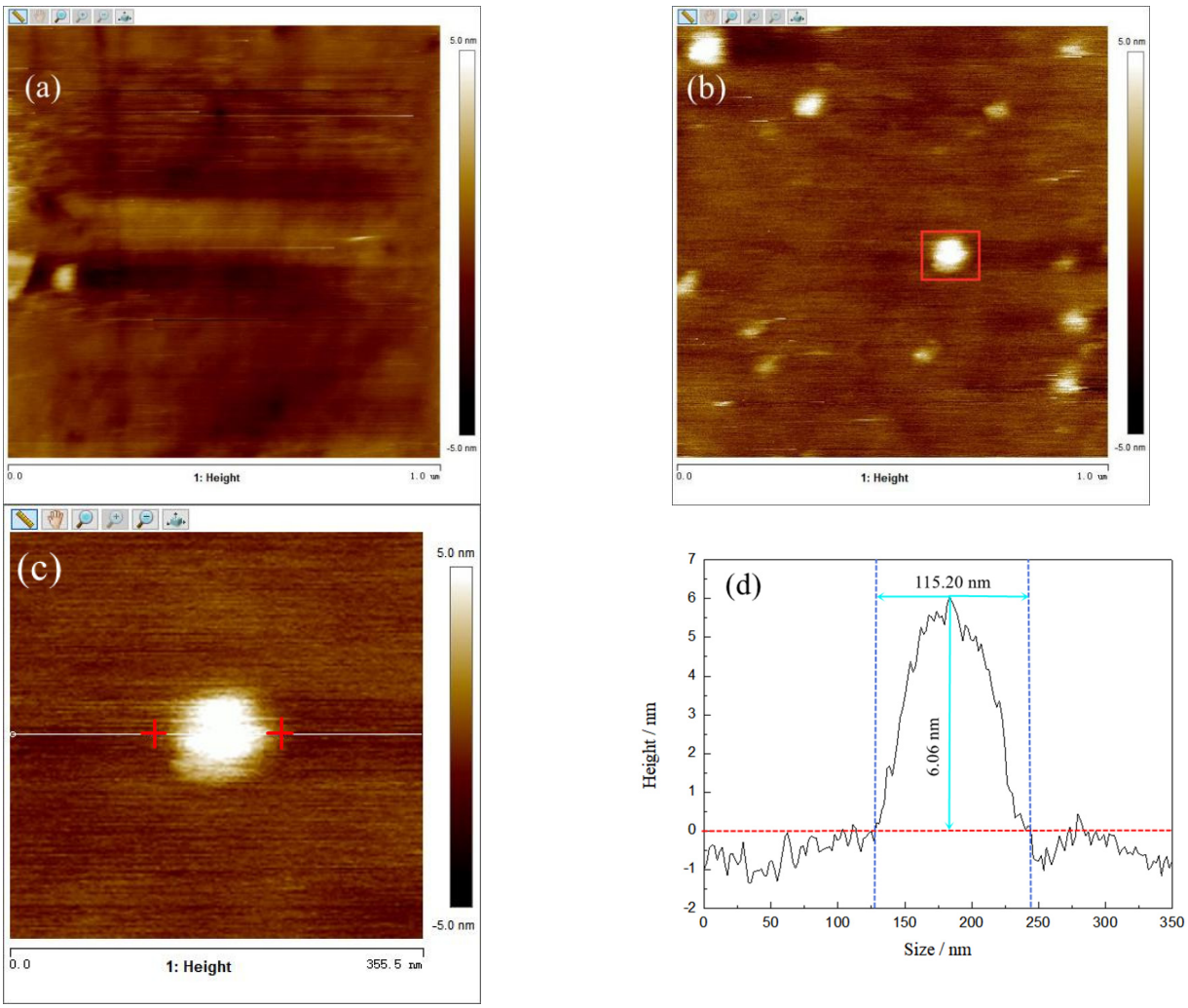
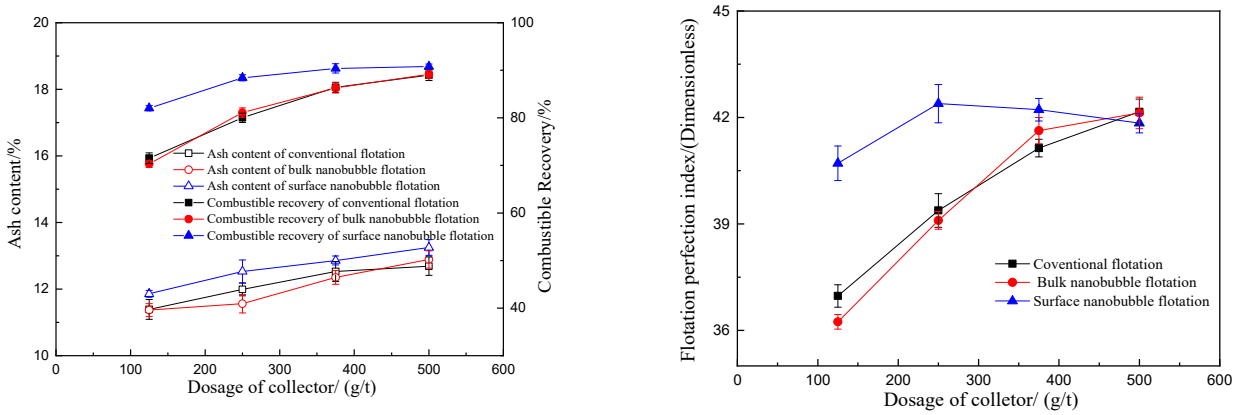



**Figure 6.** AFM image of the modified quartz surface: (**a**) fresh surface; (**b**) with hydrodynamic cavitation; (**c**) enlarged bright spot from (**b**); (**d**) Heightmap through the bright spot of (**c**) [9].

The AFM images revealed bright spots with a typical height of 6.06 nm and a diameter of 115.20 nm, consistent with the SNB morphology reported in the literature [4,20]. Although this evidence was obtained on a model substrate rather than on coal, it confirms that SNBs can stably exist on hydrophobic surfaces and supports the plausibility of SNB attachment on hydrophobic coal surfaces.

### *3.2. The Influence of Different Types of Nano-Bubbles on the Flotation of Coal Under Different Dosages of Collector*

Comparative flotation tests were conducted at kerosene dosages ranging from 125 to 500 g/t to evaluate the roles of bulk nanobubbles (BNBs) and surface nanobubbles (SNBs), and the results are presented in Figure 7. Both combustible recovery and clean coal ash increased with collector dosage across all systems, consistent with enhanced particle hydrophobicity. Flotation performance in the presence of BNBs was nearly identical to that of conventional flotation across all dosages, indicating that BNBs generated in clean water exerted negligible synergistic effects—likely because they lacked prior contact with hydrophobic particles and failed to nucleate on coal surfaces during the short conditioning period.




(**a**) (**b**)

**Figure 7.** The flotation performance between bulk and surface nonobubbles of coal flotation under various kerosene dosage: (**a**) ash content and combustible recovery of clean coal; (**b**) flotation efficiency index of clean coal.

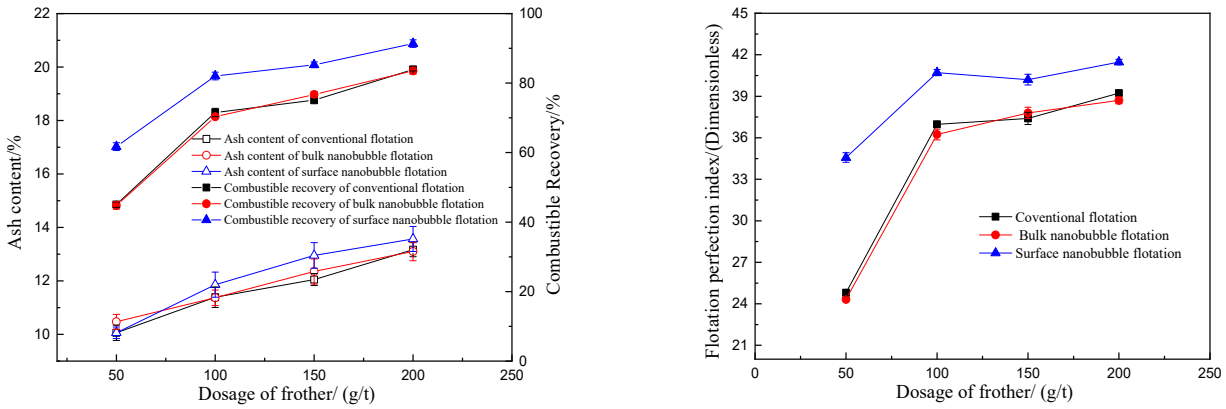
In contrast, SNBs produced a notable improvement, particularly at low collector dosages. At 125 g/t kerosene, SNB flotation increased combustible recovery from 71.52 ± 1.11% to 82.03 ± 0.55% (a gain of 10.51 percentage points), while the ash content increased only slightly from 11.39 ± 0.30% to 11.86 ± 0.10%. Statistical analysis confirmed that this increase was significant ($p < 0.05$). This improvement is likely attributable to SNBs acting as "secondary collectors" [15,20] and promoting particle aggregation via capillary bridging [12,13], thereby compensating for insufficient collector coverage. The enhancement diminished progressively with increasing collector dosage; at 500 g/t, the recovery increased from 89.00 ± 1.15% to 90.80 ± 0.51% (a gain of 1.80 percentage points), and the difference was no longer statistically significant. This diminishing trend is likely due to approaching saturation of the coal surface sites available for hydrophobic modification, as indicated by the flotation recovery data: at 500 g/t, conventional flotation already achieved a recovery close to its maximum, leaving limited room for further improvement by SNBs. Importantly, at equivalent combustible recovery, SNB flotation can reduce kerosene consumption by approximately 50% compared to conventional flotation.

### *3.3. The Influence of Different Types of Nano-Bubbles on the Flotation of Coal Under Different Dosages of Frother*

The general trends observed in Figure 8 indicate that increasing frother dosage from 50 to 200 g/t led to higher clean coal ash, combustible recovery, and flotation efficiency index across all flotation configurations, with the steepest gains occurring between 50 and 100 g/t. Beyond this point, the improvements became less pronounced, suggesting that frother adsorption approached saturation. Since bulk nanobubble concentration increases with n-octanol dosage, varying frother levels simultaneously modulated BNB concentration in the pulp. Nevertheless, BNB-assisted flotation closely paralleled conventional flotation across the entire dosage range, yielding virtually indistinguishable flotation indicators at all frother levels—a finding that reinforces the limited role of pre-formed BNBs in this system.

By contrast, the picture changed markedly when interfacial nanobubbles were present. Under SNB flotation, all indicators were consistently superior to conventional flotation, with the most striking gains observed at the lowest frother dosage. At 50 g/t n-octanol, SNBs increased combustible recovery from 45.03 ± 0.77% to 61.71 ± 0.49% (a gain of 16.68 percentage points), while the ash content remained essentially unchanged (10.06 ± 0.21% vs. 10.06 ± 0.29%). As the frother dosage rose to 200 g/t, the recovery

increased from 83.95 ± 0.47% to 91.35 ± 0.27% (a gain of 7.40 percentage points), accompanied by a modest ash increase from 13.17 ± 0.26% to 13.57 ± 0.47%. A similar pattern emerged for the flotation efficiency index: at 50 g/t n-octanol, SNBs boosted this index from 24.80 ± 0.22% to 34.57 ± 0.35% (a gain of 9.77 percentage points), whereas at 200 g/t, the improvement narrowed to 2.24 percentage points (39.23 ± 0.12% vs. 41.47 ± 0.20%). Statistical analysis confirmed that the increases in combustible recovery and flotation efficiency index induced by SNBs were significant at all frother dosages ($p < 0.05$), while ash content showed no significant difference among the three systems. These observations collectively suggest that SNBs enhance coal flotation primarily when frother is insufficient—likely by stabilizing the froth phase and facilitating bubble–particle attachment [8]. In contrast, BNBs, regardless of frother concentration, appear to offer little benefit.




(**a**) (**b**)

**Figure 8.** The flotation performance between bulk and surface nonobubbles of coal flotation under various frother dosage: (**a**) ash content and combustible recovery of clean coal; (**b**) flotation efficiency index of clean coal.

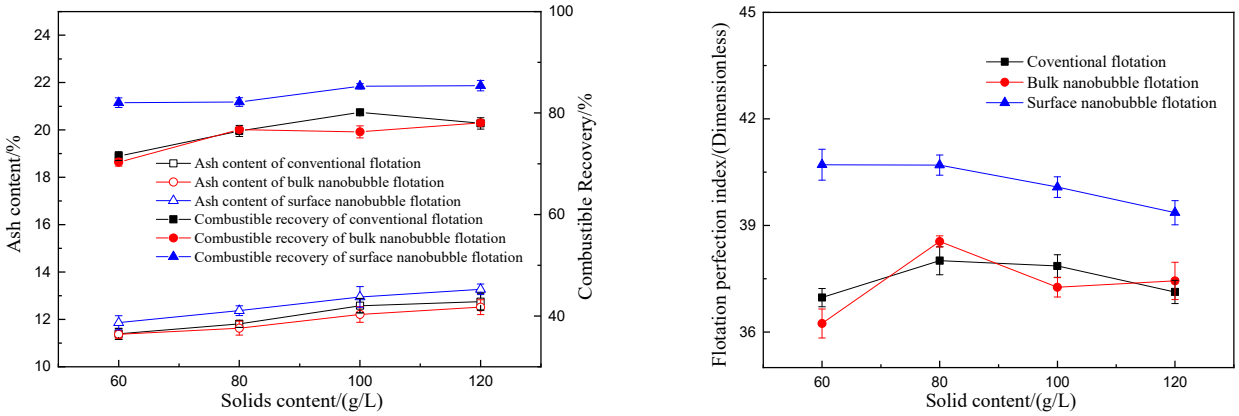
### *3.4. The Influence of Different Types of Nano-Bubbles on the Flotation of Coal Under Different Pulp Concentrations*

The effect of pulp concentration on flotation performance was evaluated under three flotation configurations, and the results are summarized in Figure 9. Across all flotation configurations, both clean coal ash and combustible recovery were lower at dilute pulp conditions than at higher concentrations. This trend can be rationalized from two perspectives: first, with reagent dosages held constant, increasing pulp concentration effectively raises the reagent dosage per unit mass of solids, thereby promoting more complete particle hydrophobization. Second, denser pulps tend to exacerbate mechanical entrainment of fine gangue particles, which inevitably report to the concentrate and elevate ash content.

When the three flotation systems were compared, BNB-enhanced flotation again yielded indicators closely resembling those of conventional flotation across all concentration levels. This consistent pattern—observed under varying collector dosages, frother levels, and pulp concentrations—strongly suggests that bulk nanobubbles, when introduced as a pretreatment step, contribute negligibly to coal flotation performance, regardless of the operating conditions examined.

In contrast, interfacial nanobubbles delivered a clear and consistent improvement across the entire pulp concentration range. At 60 g/L, SNB flotation increased combustible recovery from 71.52 ± 0.86% to 82.03 ± 0.95% (a gain of 10.51 percentage points), while ash content remained nearly unchanged (11.39 ± 0.23% vs. 11.86 ± 0.30%). As pulp concentration increased to 120 g/L, the recovery gain narrowed to 7.43 percentage points (77.96 ± 1.11% vs. 85.39 ± 1.02%), accompanied by a slight ash increase. Statistical analysis

confirmed that SNB flotation significantly increased combustible recovery and flotation efficiency index compared with conventional and BNB flotation at all pulp concentrations ($p < 0.05$), whereas ash content showed no significant difference among the three systems. Notably, the flotation efficiency index increased from approximately 37% for conventional flotation to around 40% for SNB flotation. It is worth noting, however, that further increases in pulp concentration led to a reduction in clean coal ash content and a corresponding decline in separation efficiency—a trend more pronounced in SNB flotation than in the other two systems. This deterioration likely reflects overloading of the froth phase with fine solids at high slurry densities, which undermines the selectivity gains otherwise provided by surface nanobubbles.




(**a**) (**b**)

**Figure 9.** The flotation performance between bulk and surface nonobubbles of coal flotation under various solids content: (**a**) ash content and combustible matter recovery of clean coal; (**b**) flotation efficiency index of clean coal.

### *3.5. Comparison of Coal Flotation Kinetics Results Under Different Types of Nanobubbles*

To further quantify the differences among the three flotation systems, kinetic experiments were conducted under fixed reagent dosages (kerosene: 125 g/t, n-octanol: 100 g/t) and pulp concentration (60 g/L). These conditions were selected based on the preceding optimization tests, where the enhancement effect of SNBs was most pronounced at relatively low collector and frother levels. For BNB tests, the bulk nanobubble concentration was maintained at approximately $5 \times 10^7$ particles/mL; for SNB tests, the optimal cavitation parameters identified in previous experiments were applied. Froth products were sequentially collected at eight time intervals: 0–15 s, 15–30 s, 30–45 s, 45–60 s, 60–90 s, 90–120 s, 120–180 s, and 180–300 s. Each concentrate fraction was filtered, dried, weighed, and assayed for ash content.

The classical first-order kinetic model, which has been widely used to describe flotation processes, was employed to fit the experimental data:

$$\varepsilon = \varepsilon_\infty[1 - \exp(-kt)] \quad (1)$$

where $\varepsilon$ is the actual combustible recovery (%), $\varepsilon_\infty$ represents the theoretical maximum recovery (%), k is the flotation rate constant ($min^{-1}$), and t represents the flotation time (min). The model fits were evaluated by correlation coefficients ($R^2 > 0.98$ for all cases), confirming its suitability for describing the kinetic behavior in this study.

As shown in Figure 10, the combustible recovery increased monotonically with flotation time across all three systems, approaching a plateau at approximately 3 min. Beyond this point, further flotation yielded negligible additional recovery, indicating that the read-

ily floatable components had been largely recovered. Notably, the initial flotation rates (within the first 0.75 min) differed markedly among the three systems: SNB flotation exhibited the steepest rise, followed by BNB flotation, while conventional flotation showed the slowest recovery build-up, suggesting that nanobubbles—particularly SNBs—accelerated the early-stage collection of coal particles.

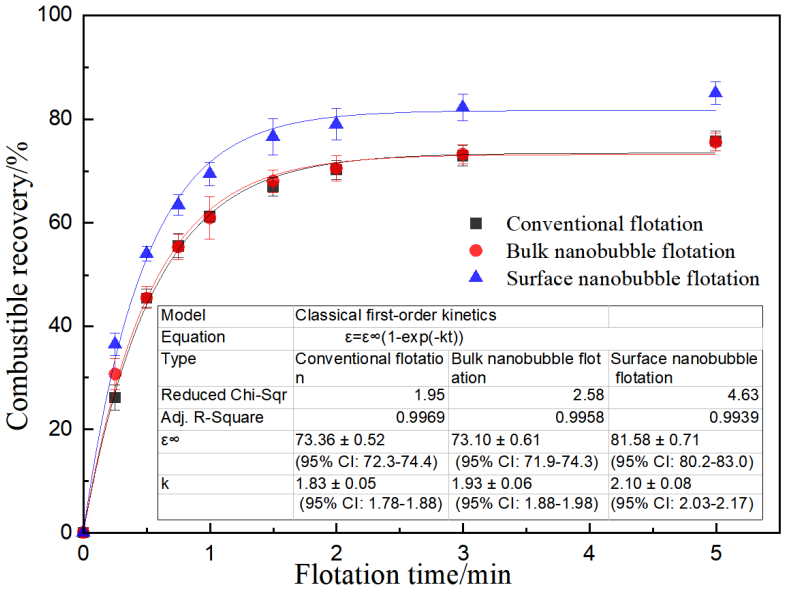



**Figure 10.** The effect of different types of nanobubbles on coal flotation kinetics.

The fitted kinetic parameters further substantiate this observation. The flotation rate constants were 1.83 ± 0.05 $min^{-1}$ for conventional flotation, 1.93 ± 0.06 $min^{-1}$ for BNB flotation, and 2.10 ± 0.08 $min^{-1}$ for SNB flotation, with 95% confidence intervals of [1.78, 1.88], [1.88, 1.98], and [2.03, 2.17] $min^{-1}$, respectively. One-way ANOVA followed by Tukey's post hoc test showed that the k value for SNB flotation was significantly higher than those for conventional and BNB flotation ($p < 0.05$), while no significant difference was found between conventional and BNB flotation ($p > 0.05$). Similarly, the fitted ultimate recovery (ε∞) for SNB flotation reached 81.58 ± 0.71% (95% CI: 80.2–83.0%), compared with 73.36 ± 0.52% (95% CI: 72.3–74.4%) for conventional flotation and 73.10 ± 0.61% (95% CI: 71.9–74.3%) for BNB flotation. The difference between SNB and the other two systems was statistically significant ($p < 0.05$). Error bars in Figure 10 represent the standard deviation of three independent replicates, and different letters indicate significant differences among flotation systems ($p < 0.05$).

The enhanced flotation kinetics observed with SNBs is likely attributable to two synergistic factors: (i) SNBs likely act as secondary collectors that increase particle surface hydrophobicity [15,20], and (ii) the capillary bridging between adjacent particles induced by SNBs generates hydrophobic aggregates with larger apparent sizes [12,13], thereby improving the collision and attachment probabilities with rising bubbles [3]. These combined effects not only accelerate the flotation process but also enhance the fitted ultimate recovery of combustible materials, which aligns well with the improved performance observed in the preceding batch flotation tests. In contrast, the marginal improvement offered by BNBs suggests that bulk nanobubbles, which lack effective anchoring on particle surfaces, contribute little to either flotation kinetics or recovery.

### *3.6. The Influence of Nanobubbles on the Hydrophobicity of Mineral Surfaces*

To investigate the effect of nanobubbles on surface wettability, contact angle measurements were performed using the captive bubble method on hydrophobized smooth glass

surfaces with three distinct wettability levels: weakly hydrophobic (approximately 30°), moderately hydrophobic (approximately 60°), and strongly hydrophobic (approximately 90°). Hydrophobized glass slides were used rather than coal because coal surfaces are heterogeneous and rough, leading to poorly reproducible contact angles. Smooth model substrates with controlled wettability allow systematic investigation of nanobubble behavior as a function of surface hydrophobicity. Each substrate was tested under three conditions: conventional (without nanobubbles), BNB treatment, and SNB treatment. The measured contact angles are presented in Figure 11.

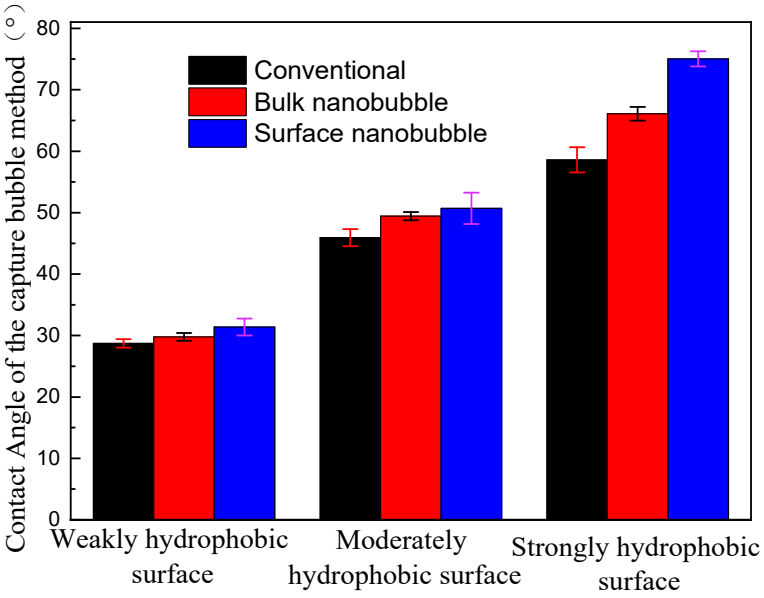



**Figure 11.** Contact angle of different hydrophobic samples under treatments of different nanobubble types.

As shown in Figure 11, the contact angle values for all substrates increased to varying extents following nanobubble treatment compared to the conventional condition. For the weakly hydrophobic substrate (approximately 30°), SNB treatment increased the contact angle from 28.73 ± 0.68° to 31.39 ± 1.38° ($p < 0.05$), while BNB showed no significant difference from the control (29.78 ± 0.62°). For the moderately hydrophobic substrate (approximately 60°), SNB again yielded a significant increase (50.70 ± 2.54° vs. 45.94 ± 1.41° for the control, $p < 0.05$), whereas BNB (49.44 ± 0.67°) was not significantly different from either. For the strongly hydrophobic substrate (approximately 90°), all three treatments differed significantly ($p < 0.05$): conventional 58.59 ± 2.06°, BNB 66.10 ± 1.11°, and SNB 75.04 ± 1.23°. The corresponding 95% confidence intervals were [27.76, 29.70]°, [28.90, 30.66]°, and [29.44, 33.34]° for the weakly hydrophobic substrate; [43.95, 47.93]°, [48.50, 50.38]°, and [47.11, 54.29]° for the moderately hydrophobic substrate; and [55.69, 61.49]°, [64.52, 67.68]°, and [73.30, 76.78]° for the strongly hydrophobic substrate.

These results show that both BNB and SNB treatments enhanced surface hydrophobicity, with SNBs consistently producing greater improvements than BNBs. Interestingly, despite the negligible role of BNBs in coal flotation observed in earlier sections, they still measurably increased the contact angles of the model substrates, suggesting that the mere presence of BNBs can modify local interfacial properties even if their macroscopic flotation effect is minimal. It should be noted that contact angles were measured under static conditions on model substrates. While BNBs can increase the contact angle on such surfaces, their attachment to real coal particles under dynamic flotation conditions is weak. SNBs, however, are directly nucleated on particle surfaces and remain stable, thereby contributing to flotation.

### *3.7. The Influence of Nano-Bubbles on the Agglomeration of Fine Coal Particles*

To elucidate the role of nanobubbles in particle–particle interactions, agglomeration behavior of fine coal particles with different densities was examined under three pretreatment conditions: deionized water, BNBs, and SNBs. The observed agglomeration morphologies are presented in Figure 12.

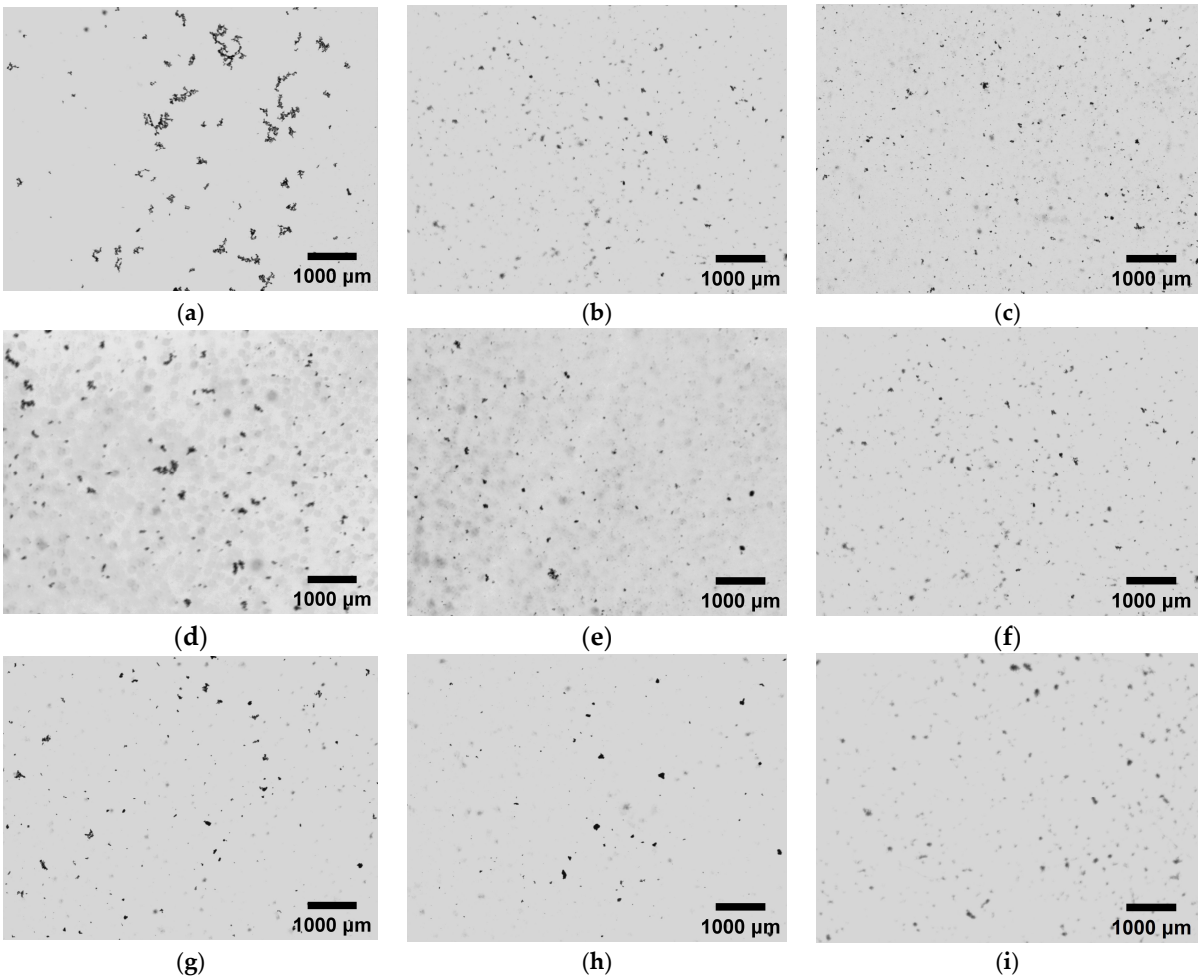



**Figure 12.** The aggregation behavior of different density fine coal under different nanobubble type: (**a**) surface nanobubble and high-density fine coal; (**b**) surface nanobubble and medium-density fine coal; (**c**) surface nanobubble and low-density fine coal; (**d**) bulk nanobubble and high-density fine coal; (**e**) bulk nanobubble and medium-density fine coal; (**f**) bulk nanobubble and low-density fine coal; (**g**) deionized water and high-density fine coal; (**h**) deionized water and medium-density fine coal; (**i**) deionized water and low-density fine coal.

Regardless of the pretreatment condition, low-density coal exhibited the strongest agglomeration, followed by medium-density coal, while high-density coal showed the least tendency to form aggregates. This trend is consistent with the decreasing surface hydrophobicity as particle density increases. It should be noted that density and ash content are inherently coupled in coal; the density fractions used here inevitably differ in mineralogical composition. The density fractionation was therefore employed to obtain samples with varying surface hydrophobicity rather than to isolate density as an independent variable. To provide quantitative support, the agglomeration images were analyzed using ImageJ software (version 1.54g). The equivalent diameter of each aggregate was calculated as:

$$D_{eq} = 2\sqrt{Area/\pi} \quad (2)$$

The number-based $D_{10}$, $D_{50}$, and $D_{90}$ values are summarized in Table 5. For low-density coal (−1.4 g/cm$^3$), SNB treatment produced the largest aggregates ($D_{50}$ = 72.57 μm, $D_{90}$ = 159.98 μm), followed by BNB ($D_{50}$ = 54.69 μm, $D_{90}$ = 139.32 μm) and the deionized water control ($D_{50}$ = 35.68 μm, $D_{90}$ = 84.47 μm). A similar but less pronounced trend was observed for medium-density coal (1.4–1.8 g/cm$^3$), with SNB again yielding larger aggregates than BNB and the control. In contrast, for high-density coal (+1.8 g/cm$^3$), neither BNB nor SNB treatment increased the aggregate size relative to the control. These quantitative results confirm that SNBs are more effective than BNBs in promoting the agglomeration of low-density coal particles, while high-density hydrophilic particles show negligible response.

**Table 5.** Agglomerate size distribution ($D_{10}$, $D_{50}$, $D_{90}$) of fine coal particles with different density fractions after conventional, BNB, and SNB treatments.

| Densimetric Fraction (g/cm$^3$) | Treatment | $D_{10}$ (μm) | $D_{50}$ (μm) | $D_{90}$ (μm) |
|---|---|---|---|---|
| −1.4 g | Conventional | 19.54 | 35.68 | 84.47 |
| | BNBs | 17.02 | 54.69 | 139.32 |
| | SNBs | 21.63 | 72.57 | 159.98 |
| 1.4–1.8 | Conventional | 16.93 | 32.90 | 84.22 |
| | BNBs | 16.93 | 35.46 | 79.94 |
| | SNBs | 19.54 | 55.85 | 129.70 |
| +1.8 | Conventional | 11.28 | 38.68 | 82.92 |
| | BNBs | 19.54 | 33.85 | 71.81 |
| | SNBs | 16.93 | 31.41 | 64.08 |

These observations suggest that the agglomeration-strengthening effect of nanobubbles is fundamentally dependent on particle surface hydrophobicity. The superior performance of SNBs over BNBs in promoting agglomeration can be rationalized by the fact that SNBs are pre-nucleated directly on particle surfaces during cavitation, where they serve as effective bridging agents between adjacent hydrophobic particles. The capillary interaction forces arising from these surface-attached nanobubbles, together with the enhanced surface hydrophobicity, are likely the primary contributors to the increased degree of aggregation and aggregate stability observed in SNB-treated low-density coal slurries. Within the framework of extended DLVO theory, these capillary and hydrophobic interactions reduce the interfacial free energy and lower the energy barrier for particle–particle attachment, which is consistent with the larger $D_{50}$ and $D_{90}$ values observed for SNB-treated low-density coal. In contrast, the weaker aggregation effect of BNBs can be attributed to their lower stability on particle surfaces. Under shear forces in the flotation pulp, BNBs are readily detached and cannot sustain this interfacial modification, whereas SNBs remain firmly anchored and maintain capillary bridging, leading to more stable aggregates.

## 4. Conclusions

This study systematically compared the roles of bulk nanobubbles (BNBs) and surface nanobubbles (SNBs) in fine coal flotation using a unified hydrodynamic cavitation platform. The results establish a clear functional distinction between the two bubble types. BNBs—generated in clean water and introduced to the pulp as a separate stream—showed no significant improvement in flotation performance across all tested conditions, regardless of collector dosage, frother level, or pulp concentration. In contrast, SNBs produced directly on particle surfaces by cavitating the coal slurry significantly enhanced combustible recovery, particularly at low reagent dosages. At 125 g/t kerosene, combustible recovery increased by 10.51 percentage points, and at 50 g/t n-octanol, the gain reached 16.68 per-

centage points. Notably, SNB flotation achieved comparable performance to conventional flotation using approximately 50% less collector, highlighting its practical potential for reducing reagent consumption in industrial operations.

Mechanistically, the superiority of SNBs likely stems from their direct nucleation on hydrophobic particle surfaces, where they may act as secondary collectors and promote particle aggregation through capillary bridging forces. This dual function enhances both surface hydrophobicity and apparent particle size, thereby improving the collision and attachment with rising bubbles. The density-dependent agglomeration behavior further supports that the strengthening effect is fundamentally governed by particle surface hydrophobicity. An intriguing discrepancy emerged from the contact angle measurements: although BNBs measurably increased hydrophobicity on model substrates, this effect did not translate into improved flotation in real slurries—likely because BNBs lack sufficient opportunity to anchor on particles under actual flotation conditions. Overall, this work provides evidence that SNBs, rather than BNBs, are likely the primary driver of enhanced flotation performance. Future efforts should focus on optimizing cavitation parameters to maximize SNB formation on target minerals and extending this approach to other fine particle systems where flotation efficiency remains a challenge.

**Author Contributions:** Conceptualization, H.H.; methodology, H.H. and B.Y.; investigation, X.Z.; date curation, X.Z. and Y.L.; Supervision, B.Y.; funding acquisition, Y.L. and H.H.; writing—original draft preparation, H.H. and X.Z.; visualization, W.M. and W.L. All authors have read and agreed to the published version of the manuscript.

**Funding:** This research was supported by Hebei Natural Science Foundation (Grant No. E2025403025), the Science Research Project of Hebei Education Department (Grant No. QN2024214), the Open Fund of Engineering Research Center for Silicate Solid Waste Resource Utilization of Hebei Province (Grant No. Z2026003), and the Doctoral Scientific Research Startup Fund of Hebei GEO University (Grant No. BQ2026086).

**Data Availability Statement:** The original contributions presented in this study are included in the article. Further inquiries can be directed to the corresponding author.

**Conflicts of Interest:** The authors declare no conflicts of interest.

## References

1. Heidari, H.; Azizi, A.; Hassanzadeh, A. A new insight into the mechanism of MNB-assisted flotation of copper: A link between chalcopyrite and its-bearing bulk ore. *Miner. Eng.* **2024**, *216*, 108882. [CrossRef]
2. Cotrina-Teatino, M.A.; Marquina-Araujo, J.J.; Contreras-Valverde, J.S.; Valdivieso-Saavedra, M.A. Nanobubbles and the flotation process in mineral recovery: A bibliometric and systematic literature analysis covering the period 2005–2024. *Miner. Eng.* **2025**, *227*, 109310. [CrossRef]
3. Jiang, H.Y.; Yang, H.C.; Xing, Y.W.; Cao, Y.J.; Gui, X.H. The effect of impeller speeds on the nanobubbles flotation efficiency of ultrafine coal particles. *Powder Technol.* **2025**, *449*, 120431. [CrossRef]
4. Li, C.W.; Zhang, H.J. A review of bulk nanobubbles and their roles in flotation of fine particles. *Powder Technol.* **2022**, *395*, 618–633. [CrossRef]
5. Zhang, X.; Wang, Q.; Wu, Z.; Tao, D. An experimental study on size distribution and zeta potential of bulk cavitation nanobubbles. *Int. J. Miner. Metall. Mater.* **2020**, *27*, 152–161. [CrossRef]
6. Montazeri, S.M.; Kalogerakis, N.; Kolliopoulos, G. Effect of chemical species and temperature on the stability of air nanobubbles. *Sci. Rep.* **2023**, *13*, 16716. [CrossRef] [PubMed]
7. Ahmadi, R.; Khodadadi, D.A.; Abdollahy, M.; Fan, M.M. Nano-microbubble flotation of fine and ultrafine chalcopyrite particles. *Int. J. Min. Sci. Technol.* **2014**, *24*, 559–566. [CrossRef]
8. Qiao, B.; Wu, Z.X.; Liu, Y.; Chen, R.F.; Ran, J.C.; Tao, D.P. Effects of nanobubbles on flotation froth characteristics and associated mechanisms. *Colloids Surf. Physicochem. Eng. Asp.* **2026**, *728*, 138564. [CrossRef]
9. Han, H.; Liu, A.; Wang, C.; Yang, R.; Li, S.; Wang, H. Flotation kinetics performance of different coal size fractions with nanobubbles. *Int. J. Miner. Metall. Mater.* **2022**, *29*, 1502–1510. [CrossRef]

10. Ma, F.Y.; Zhang, D.; Tao, D.P. Study on Flotation Behavior of Fine Flake Graphite Enhanced by Nanobubbles. *Nanomaterials* **2025**, *15*, 1542. [CrossRef] [PubMed]
11. Sobhy, A.; El-Shamy, H.; Ahmed, N.; Farahat, M. Nanobubble flotation strategy of fluorite integrating experimental and DFT analysis. *Adv. Colloid Interface Sci.* **2026**, *352*, 103833. [CrossRef] [PubMed]
12. Hampton, M.A.; Nguyen, A.V. Nanobubbles and the nanobubble bridging capillary force. *Adv. Colloid Interface Sci.* **2010**, *154*, 30–55. [CrossRef] [PubMed]
13. Knüpfer, P.; Ditscherlein, L.; Peuker, U.A. Nanobubble enhanced agglomeration of hydrophobic powders. *Colloids Surf. Physicochem. Eng. Asp.* **2017**, *530*, 117–123. [CrossRef]
14. Tao, D.P.; Sobhy, A. Nanobubble effects on hydrodynamic interactions between particles and bubbles. *Powder Technol.* **2019**, *346*, 385–395. [CrossRef]
15. Yang, H.C.; Li, Y.P.; Xing, Y.W.; Cao, Y.J.; Gui, X.H. New picture on nanobubble-induced interparticle bridging: Flash expansion of gas bridges. *Miner. Eng.* **2025**, *230*, 109411. [CrossRef]
16. Tao, D.P. Recent advances in fundamentals and applications of nanobubble enhanced froth flotation: A review. *Miner. Eng.* **2022**, *183*, 107554. [CrossRef]
17. Zhou, S.Q.; Li, Y.; Nazari, S.; Bu, X.N.; Hassanzadeh, A.; Ni, C.; He, Y.Q.; Xie, G.Y. An Assessment of the Role of Combined Bulk Micro- and Nano-Bubbles in Quartz Flotation. *Minerals* **2022**, *12*, 944. [CrossRef]
18. Dutta, N.; Sharma, H.; Yadav, G.; Nirmalkar, N.; Mitra, S. Understanding the role of nanobubbles on reducing collector and frother dosages in fine particle flotation. *Sep. Purif. Technol.* **2025**, *378*, 134519. [CrossRef]
19. Qiao, B.; Wu, Z.X.; Huang, H.; Ran, J.C.; Ma, G.X.; Shao, H.Z.; Tao, D.P. An investigation of nanobubble treatment on fine particle flotation and associated mechanisms. *Green Smart Min. Eng.* **2025**, *2*, 32–41. [CrossRef]
20. Zhang, F.F.; Cai, H.J.; Fan, G.X.; Gui, X.H.; Xing, Y.W.; Cao, Y.J. The role of interfacial nanobubbles in the flotation performance of microfine particles. *Colloids Surf. Physicochem. Eng. Asp.* **2024**, *699*, 134633. [CrossRef]
21. Zhang, F.F.; Xing, Y.W.; Chang, G.H.; Yang, Z.L.; Cao, Y.J.; Gui, X.H. Enhanced lignite flotation using interfacial nanobubbles based on temperature difference method. *Fuel* **2021**, *293*, 120313. [CrossRef]
22. Wang, X.; Yuan, S.; Liu, J.; Zhu, Y.M.; Han, Y.X. Nanobubble-enhanced flotation of ultrafine molybdenum and the associated mechanism. *J. Mol. Liq.* **2022**, *346*, 118312. [CrossRef]
23. Ren, L.Y.; Zhang, X.Y.; Liu, J.; Huang, L.Y.; Bao, S.X.; Zhang, Y.M.; Nguyen, A.V. Interfacial gas enrichment mechanism for enhancing selective separation of fine particles using nano-microbubble technology. *Sep. Purif. Technol.* **2025**, *362*, 131527. [CrossRef]
24. Zhang, Z.Y.; Ren, L.Y.; Zhang, Y.M. Role of nanobubbles in the flotation of fine rutile particles. *Miner. Eng.* **2021**, *172*, 107140. [CrossRef]
25. Ren, L.Y.; Zhang, Z.Y.; Zeng, W.N.; Zhang, Y.M. Adhesion between nanobubbles and fine cassiterite particles. *Int. J. Min. Sci. Technol.* **2023**, *33*, 503–509. [CrossRef]
26. Ge, W.C.; Guo, Z.X.; Liu, J.; Chang, T.J.; Tao, Y.Y.; Zhu, Y.M.; Li, Y.J.; Yuan, S.; Li, W.B. Mechanism of enhanced flotation separation of chlorite from hematite by synergistic action of reagents and micro-nano bubbles. *Colloids Surf. Physicochem. Eng. Asp.* **2025**, *725*, 137726. [CrossRef]
27. Zhang, F.F.; Dong, W.C.; Cai, H.J.; Zhang, H.Y.; Fan, X.B.; Kang, Y.M.; Cao, Y.J.; Fan, G.X. Cavitation nanobubbles enhancing the flotation of microfine ilmenite and associated fundamentals. *Miner. Eng.* **2025**, *120*, 107510. [CrossRef] [PubMed]


**Disclaimer/Publisher's Note:** The statements, opinions and data contained in all publications are solely those of the individual author(s) and contributor(s) and not of MDPI and/or the editor(s). MDPI and/or the editor(s) disclaim responsibility for any injury to people or property resulting from any ideas, methods, instructions or products referred to in the content.